ACS OMEGA

Open Access

http://pubs.acs.org/journal/acsodf

Article

Determining the Out-of-Plane Longitudinal Sound Speed in GeS by Broadband Time-Domain Brillouin Scattering

Watheq Al-Basheer,* Christian Viernes, Meixin Cheng, Ruofei Zheng, Sam Netzke, Kostyantyn Pichugin, and German Sciaini*

Cite This: *ACS Omega* 2024, 9, 15463−15467

Read Online

ACCESS | Metrics & More | Article Recommendations

ABSTRACT: Over the past decade, two-dimensional (2D) layered semiconducting materials, with their distinctive structures and unique physicochemical properties, have attracted attention for potential applications in photonics and optoelectronics. In this study, we utilized time-domain broadband Brillouin scattering on a single germanium monosulfide (GeS) crystal to determine the out-of-plane longitudinal sound speed, evaluated at v_L = (4035 ± 200) m/s. The reported results demonstrate the effectiveness of this nondestructive, all-optical technique for measuring the elastic properties in fragile 2D layered materials and provide the value of the out-of-plane compressive elastic constant, C = (69 ± 7) GPa.

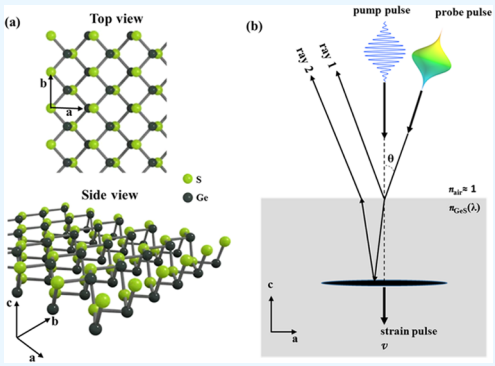

I. INTRODUCTION

The constant progress in the generation of intense and ultrashort laser pulses,[1−4] as well as rapid enhancements in various pump−probe spectroscopy techniques, has led to numerous innovative schemes for the simultaneous generation and detection of coherent acoustic phonons across a range of materials that have been used in many applications.[5−20] The generation of coherent acoustic waves by the absorption of ultrashort laser pulses, and their subsequent detection by time-delayed ultrashort probe pulses, dates back to the 1980s and gave birth to the field of picosecond ultrasonics.[5,6] Coherent acoustic phonons, produced using ultrashort pump laser pulses, have been observed to propagate through both opaque and transparent materials.[9−15] A variation of picosecond ultrasonics, which detects coherent acoustic pulses propagating in transparent media, has been termed time-domain Brillouin scattering (TDBS) because the photoelastic interaction fulfills the conditions for Brillouin scattering (BS).[21]

The impulsive thermal disruption, triggered by the absorption of an intense excitation laser pulse on a material's surface, leads to the generation of a coherent acoustic pulse.[22−26] This pulse retreats from the crystal's surface and travels into the bulk at the speed of sound, altering the material's dielectric properties and acting as a moving "internal" reflective boundary for a transmitted ray.[27−30] Thus, TDBS relies on heterodyne detection, where the refracted and weakly scattered probe beam, caused by this coherent acoustic wave, interferes with the probe beam that is reflected at the air-material interface.[30]

In this work, we performed TDBS measurements on a single GeS crystal to determine the out-of-plane longitudinal sound speed, that is, the speed of a compressive wave moving perpendicular to the plane of the two-dimensional (2D) layers constituting the crystal. GeS has recently attracted considerable attention due to its 2D layered structure and remarkable semiconducting properties.[31] Furthermore, its low bandgap and high absorption coefficient have made it an ideal candidate for a variety of applications and industries, such as solar cells,[32] fast photodetectors,[33,34] gas sensors,[35,36] batteries,[37,38] and light-emitting diodes.[39] Despite numerous studies probing the structure and physicochemical properties of GeS,[40−43] information on its acoustic or elastic properties remains scarce. In fact, to the best of our knowledge, this study is the first to experimentally determine the speed of sound in GeS.

II. EXPERIMENTAL METHODS

The sample, a single bulk crystal of GeS with a purity greater than 99.995%, was procured from HQ Graphene and utilized in TDBS experiments following surface cleaning through mechanical exfoliation. GeS is recognized as a stable 2D layered semiconductor featuring an indirect bandgap of 1.65

Received: January 8, 2024
Revised: February 4, 2024
Accepted: February 28, 2024
Published: March 12, 2024

https://doi.org/10.1021/acsomega.4c00266
ACS Omega 2024, 9, 15463−15467

eV at room temperature. The used GeS crystal is of high quality with the well-known crystalline structure, which is characterized by distorted orthorhombic symmetry (space group *Pcmn* - D_2h)[44] with unit cell parameters: a = 0.4299 nm, b = 1.0481 nm, c = 0.3646 nm, and $\alpha = \beta = \gamma = 90°$.[45]

Figure 1 shows a schematic diagram of the main components of the employed experimental pump−probe setup. The setup is based on a femtosecond laser from Light Conversion (Pharos-SP, YB/KGW), which outputs 170 fs pulses at a central wavelength of 1030 nm and a repetition rate of 6 kHz. The pump laser pulses, with a wavelength of λ_{pump}= 450 nm (2.76 eV), were generated via optical parametric amplification, followed by second harmonic generation. The pump beam was modulated with a mechanical chopper operating at half the acquisition frequency to obtain differential transient reflectivity spectra. With the aid of a long focal length lens, the pump beam was focused onto the crystal's surface to a spot size of 300 μm at fwhm (full-width half-maximum). Pumping the crystal with energy greater than its bandgap proved effective, as there was no need to add an ultrathin transducing metallic layer. The broadband probe pulses were generated by directing a small portion of the fundamental laser output to pass through a 3 mm thick YAG (yttrium aluminum garnet) crystal, after which the residual 1030 nm beam was filtered out. Consequently, white light supercontinuum probe pulses with an effective spectrum covering the wavelength range of λ_{probe} = 500−950 nm were produced and employed to monitor variations in the transient reflectivity signal. A short focal length lens focused the probe beam onto the crystal surface to a spot size of about 50 μm (fwhm). An optical delay stage situated along the probe beam path was used to control the relative timing between the pump and probe pulses. The pump pulses excited the crystal by directing a focused beam to impinge perpendicularly on the crystal's flat surface while the probe beam was angled to meet the surface at an incidence angle of $\theta \approx 10°$. The transient reflectivity spectra were detected with a dispersive spectrometer and recorded at a rate of 1 kHz.

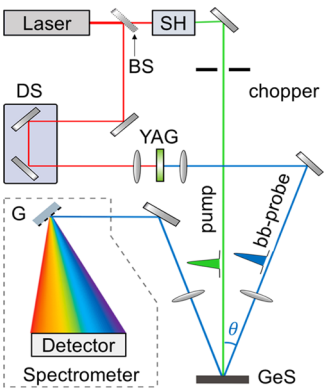

Figure 1. An experimental schematic diagram of the main components of the employed pump−probe setup. BS: beam splitter, SH: second harmonic generation, DS: optical delay stage, YAG: yttrium aluminum garnet crystal, G: grating, GeS: germanium sulfide crystal.

III. RESULTS AND DISCUSSION

The Brillouin frequency (ν_B), arising from alternating constructive and destructive interference events observed in the time domain, is given by eq 1[14,24,46]

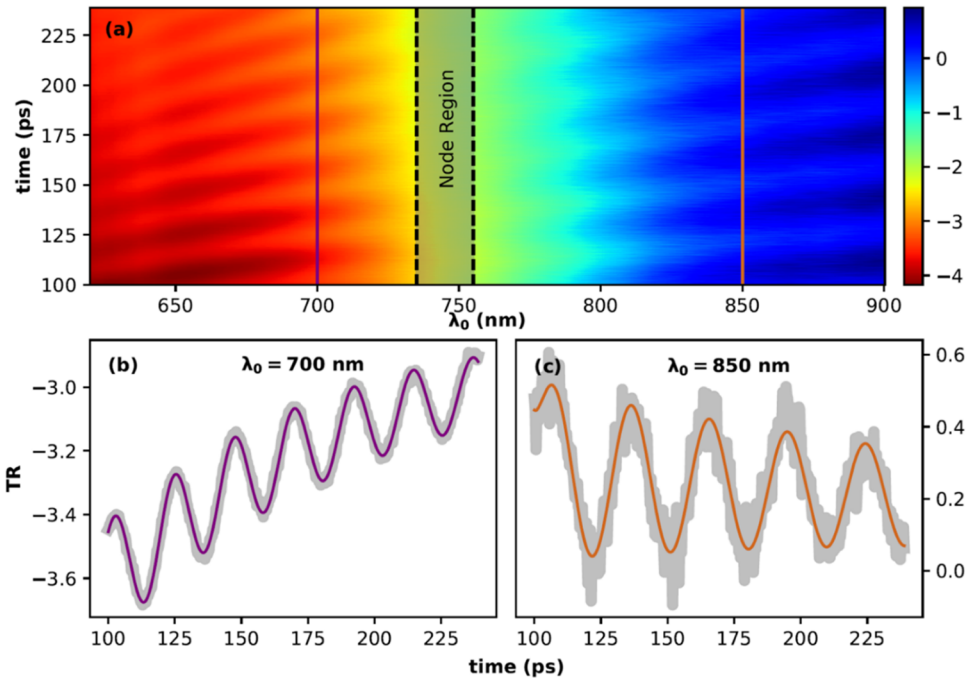

Figure 2. (a) Broadband time-resolved transient reflectivity spectrum acquired at room temperature with a time step of 300 fs, which also shows the node region extending observed over the wavelength range of 735−755 nm. Parts (b) and (c) of the figure show two expanded slices of the time-resolved broadband transient reflectivity spectrum obtained at probe wavelengths of 700 and 850 nm, respectively, with the thick gray oscillatory structures representing experimental data points. The theoretically obtained fittings were shown in parts (b) and (c) as oscillatory thin traces. The expanded slices (b) and (c) were also exhibited as the two vertical lines in the transient reflectivity spectrum of part (a).

https://doi.org/10.1021/acsomega.4c00266
ACS Omega 2024, 9, 15463−15467

$$\nu_B = 2\nu_L \frac{\sqrt{n^2 - \sin^2\theta}}{\lambda_0} \quad (1)$$

where λ_0 is the wavelength of the probe beam in air, $\nu_L$is the out-of-plane longitudinal sound velocity, and n is the real part of the crystal's refractive index. The importance of eq 1 lies in the fact that it allows for the direct extraction of ν_B from experimentally obtained time-dependent transient reflectivity profiles over the probe laser wavelength range. This valuable parameter can then be used to glean important information about the material's elastic properties. Figure 2a shows a broadband time-resolved transient reflectivity spectrum acquired at room temperature with a time step of 300 fs. A distinctive feature associated with TDBS phenomena is the long-lived oscillation, which is superimposed on a slowly varying background, resulting from the dynamics of photo-excited carriers in the GeS crystal. In addition, a nonoscillating region in the spectrum, termed as the "node region", extends from λ_0= 735 to 755 nm. The term "node" denotes a wavelength region over which a π-phase flip occurs, resulting in the absence of detectable oscillatory behavior.

The two vertical lines at λ_0= 700 and 850 nm mark specific slices of the time-resolved broadband transient reflectivity spectrum that are expanded to reveal the time traces shown in Figure 2b,2c, respectively. The thick gray traces correspond to experimentally obtained data points, while the thin solid traces represent fittings of the data that were obtained using the following phenomenological model

$$S(t) = A_1(1 - e^{-(t-t_1)/\tau_1}) + A_2 e^{-(t-t_2)/\tau_2} + A_3 e^{-(t-t_3)/\tau_3}\sin(2\pi\nu_B t + \varphi) + C \quad (2)$$

The implementation of eq 2 enables the extraction ν_B at each probe wavelength, λ_0, by incorporating various fitting parameters, where $\tau_{i=1,2,3}$ are time constants, $A_{i=1,2,3}$ are amplitudes, $t_{i=1,2,3}$ are time origins, φ is a phase shift with respect to time zero, and C is constant. The first two exponential terms were incorporated to account for the time-dependent background signal arising from carrier dynamics, which accompanied the oscillatory component of interest. The latter is represented by the sine function in the third term, which includes a damping factor to account for decoherence effects and the weak absorption experienced at probing wavelengths approaching the bandgap of GeS.

It is experimentally feasible to measure the real part of the index of refraction over the probe pulse wavelengths that are accessible. Thus, given that ν_B, $n(\lambda_0)$, and θ are known, eq 1 can establish a linear correlation when ν_B is plotted as a function $\frac{n^*}{\lambda_0} = \frac{\sqrt{n^2 - \sin^2\theta}}{\lambda_0}$, where the slope that equals $2\nu_L$. We measured the refractive index of our sample by using ellipsometry, as shown in Figure 3a. The real part of the refractive index, n (dashed light blue trace), was fitted (solid orange trace) within the 620−900 nm probe wavelength interval using the Sellmeier equation form

$$n^2(\lambda_0) = 1 + \sum_i \frac{B_i \lambda_0^2}{\lambda_0^2 - C_i} \quad (3)$$

Where B_i and C_i are the determined Sellmeier coefficients. The best fit yielded the following values of $B_{i=1,2,3}$: 4.94119359, 4.99160735, and 1.26978087, respectively, whereas the $C_{i=1,2,3}$ fitting values were determined as 82 849.3204, 82 841.1046, and 291 186.190, respectively. We preferred the Sellmeier equation for fitting the data of the real part of the refractive index because it provided a better fit than the Cauchy equation. Using the imaginary part value of the refractive index k = 1.9 at λ_{pump}= 450 nm, we evaluated the optical absorption depth as $\delta = \frac{\lambda_{pump}}{4\pi k}$ = 19 nm from the crystal's interface. Such a shallow optical penetration depth ensures a more precisely defined coherent acoustic pulse.

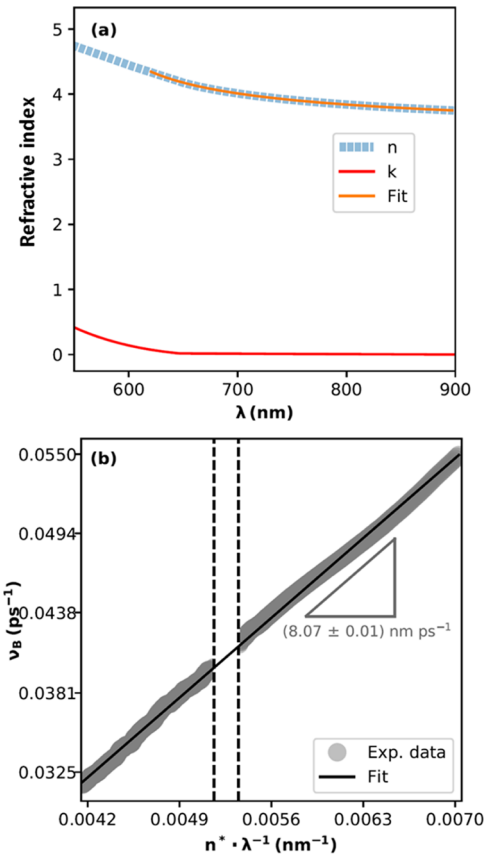

Figure 3. (a) Real (n) and imaginary (k) parts of the refractive index of GeS as a function of wavelength. Also, the fitting of the real part using Sellmeier eq 3 is shown as the trace over the wavelength region of 620−900 nm. Panel (b) shows the linear correlation revealed in eq 1 between Brillouin frequency ν_B and the ratio $n^*(\lambda_0)/\lambda_0$ over the broadband laser wavelength range 620−900 nm. The dark, thick region represents the progression of experimental data points, whereas the linear fitting is shown as the thin black trace, which has a slope of $2\nu_L$= 8.07 nm/ps (8070 m/s). The node region is shown between the two vertical dashed lines.

Figure 3b exhibits the linear correlation obtained when plotting ν_B as a function of $\frac{n^*}{\lambda_0}$. It is important to note that eq 1 was derived using the standard beam propagation model,[47] which posits that n determines the direction of the refracted probe ray, while k is accounted for as an attenuation affecting its amplitude. Chang et al.[47] defined the limiting condition for the accurate use of this model as a k/n ratio of less than 0.07. This supports our choice of the 620−900 nm probe pulse wavelength region, where the k/n ratio was below 0.05. As previously mentioned, the slope of the linear fit, corresponding to $2\nu_L$= 8070 m/s, yields a longitudinal sound speed in the GeS crystal along the out-of-plane direction of ν_L= (4035 ± 200) m/s. The error bar predominantly arises from the anisotropic

https://doi.org/10.1021/acsomega.4c00266
ACS Omega 2024, 9, 15463−15467

nature of the crystal and the imprecise determination of its crystalline orientation in our TDBS and ellipsometry measurements, potentially leading to an uncertainty of approximately 5% in the relative values of n. Furthermore, the determined speed of sound is related to the compressive elastic constant $C = \rho v_L^2$, where $\rho = 4.24$ g/cm^3 is the mass density of GeS.[44] By substitution of these values, the elastic constant C was calculated to be (69 ± 7) GPa. Koc et al.[44,48] calculated a value of $C = 169.08$ GPa using first-principles, where $C = C_{22}$ according to their selection of unit cell axes. This value of C implies a sound speed of approximately 6300 m/s, leading to a relative error in the determination of the sound speed, represented by $\left|\frac{\Delta v_L}{v_L}\right|$ of 0.44 (44%). Our experimental value suggests the need for a reparameterization of the function used in first-principles calculations.

IV. CONCLUSIONS

In summary, we have successfully performed broadband TDBS measurements on a single GeS crystal and determined the out-of-plane longitudinal sound speed, v_L = (4035 ± 200) m/s, corresponding to a compressive elastic constant, C = (69 ± 7) GPa. This latter value is comparable to that recently determined for the 2D layered semiconducting material SnS_2, (39 + 3) GPa,[49] which is in reasonable agreement with the value of 32 GPa calculated by Zhen and Wang.[50] Therefore, our findings are anticipated to guide the reparameterization of the functional used in first-principles calculations for GeS or perhaps to prompt modification of the methods employed. These results underscore the effectiveness of this non-destructive, all-optical technique for studying the elastic properties of fragile two-dimensional layered materials that cannot be investigated using typical compression-based tests.

AUTHOR INFORMATION

Corresponding Authors

Watheq Al-Basheer − *Department of Physics and Interdisciplinary Research Center of Membranes and Water Security, King Fahd University of Petroleum & Minerals, Dhahran 31261, Saudi Arabia;* orcid.org/0000-0002-2100-9333; Email: watheq@kfupm.edu.sa

German Sciaini − *The Ultrafast Electron Imaging Lab, Department of Chemistry, and Waterloo Institute for Nanotechnology, University of Waterloo, Waterloo N2L 3G1, Canada;* orcid.org/0000-0002-2120-3996; Email: gsciaini@uwaterloo.ca

Authors

Christian Viernes − *The Ultrafast Electron Imaging Lab, Department of Chemistry, and Waterloo Institute for Nanotechnology, University of Waterloo, Waterloo N2L 3G1, Canada*

Meixin Cheng − *The Ultrafast Electron Imaging Lab, Department of Chemistry, and Waterloo Institute for Nanotechnology, University of Waterloo, Waterloo N2L 3G1, Canada*

Ruofei Zheng − *The Ultrafast Electron Imaging Lab, Department of Chemistry, and Waterloo Institute for Nanotechnology, University of Waterloo, Waterloo N2L 3G1, Canada*

Sam Netzke − *The Ultrafast Electron Imaging Lab, Department of Chemistry, and Waterloo Institute for Nanotechnology, University of Waterloo, Waterloo N2L 3G1, Canada*

Kostyantyn Pichugin − *The Ultrafast Electron Imaging Lab, Department of Chemistry, and Waterloo Institute for Nanotechnology, University of Waterloo, Waterloo N2L 3G1, Canada*

Complete contact information is available at: https://pubs.acs.org/10.1021/acsomega.4c00266

Notes

The authors declare no competing financial interest.

ACKNOWLEDGMENTS

W. Al-Basheer is grateful to King Fahd University of Petroleum and Minerals for funding this research under Research Grant (#ISP221-PHYS-765). G.S. acknowledges the support of the National Science and Engineering Research Council of Canada, the Canada Foundation of Innovation, the Ontario Research Foundation.

REFERENCES

(1) Fork, R. L.; Shank, C. V.; Hirlimann, C.; Yen, R.; Tomlinson, W. J. Femtosecond white-light continuum pulses. *Opt. Lett.* **1983**, *8* (1), 1−3.

(2) Knox, W. H.; Downer, M. C.; Fork, R. L.; Shank, C. V. Amplified femtosecond optical pulses and continuum generation at 5-kHz repetition rate. *Opt. Lett.* **1984**, *9* (12), 552−554.

(3) Strickland, D.; Mourou, G. Compression of Amplified Chirped Optical Pulses. *Opt. Commun.* **1985**, *56*, 219−221.

(4) Rullière, C. *Femtosecond Laser Pulses: Principles and Experiments*; Springer, 2005; pp 1−23.

(5) Nelson, K. A. Stimulated Brillouin scattering and optical excitation of coherent shear waves. *J. Appl. Phys.* **1982**, *53*, 6060−6063, DOI: 10.1063/1.331556.

(6) Thomsen, C.; Strait, J.; Vardeny, Z.; Maris, H. J.; Tauc, J.; Hauser, J. J. Coherent phonon generation and detection by picosecond light pulses. *Phys. Rev. Lett.* **1984**, *53*, 989−992.

(7) Devos, A.; Côte, R. Strong oscillations detected by picosecond ultrasonics in silicon: Evidence for an electronic-structure effect. *Phys. Rev. B* **2004**, *70*, No. 125208.

(8) Makarona, E.; Daly, B.; Im, J.-S.; Maris, H.; Nurmikko, A.; Han, J. Coherent generation of 100 GHz acoustic phonons by dynamic screening of piezoelectric fields in AlGaN/GaN multilayers. *Appl. Phys. Lett.* **2002**, *81*, 2791.

(9) Ren, Y. H.; Trigo, M.; Merlin, R.; Adyam, V.; Li, Q. Generation and detection of coherent longitudinal acoustic phonons in the $La_{0.67}Sr_{0.33}MnO_3$ thin films by femtosecond light pulses. *Appl. Phys. Lett.* **2007**, *90*, No. 251918, DOI: 10.1063/1.2751130.

(10) Matsuda, O.; Wright, O. B.; Hurley, D. H.; Gusev, V.; Shimizu, K. Coherent shear phonon generation and detection with picosecond laser acoustics. *Phys. Rev. B* **2008**, *77*, No. 224110.

(11) Harb, M.; Peng, W.; Sciaini, G.; Hebeisen, C. T.; Ernstorfer, R.; Eriksson, M. A.; Lagally, M. G.; Kruglik, S. G.; Miller, R. J. D. Excitation of longitudinal and transverse coherent acoustic phonons in nanometer free-standing films of (001) Si. *Phys. Rev. B* **2009**, *79*, No. 094301.

(12) Brivio, S.; Polli, D.; Crespi, A.; Osellame, R.; Cerullo, G.; Bertacco, R. Observation of anomalous acoustic phonon dispersion in $SrTiO_3$ by broadband stimulated Brillouin scattering. *Appl. Phys. Lett.* **2011**, *98*, No. 211907, DOI: 10.1063/1.3593488.

(13) Pontecorvo, E.; Ortolani, M.; Polli, D.; Ferretti, M.; Ruocco, G.; Cerullo, G.; Scopigno, T. Visualizing coherent phonon propagation in the 100 GHz range: A broadband picosecond acoustics approach. *Appl. Phys. Lett.* **2011**, *98*, No. 011901, DOI: 10.1063/1.3532961.

(14) Ruello, P.; Pezeril, T.; Avanesyan, S.; Vaudel, G.; Gusev, V.; Infante, I. C.; Dkhil, B. Photoexcitation of gigahertz longitudinal and shear acoustic waves in $BiFeO_3$ multiferroic single crystal. *Appl. Phys. Lett.* **2012**, *100*, No. 212906.
(15) Devos, A.; Wen, Y.-C.; Mante, P.-A.; Sun, C.-K. Comment on "Observation of anomalous acoustic phonon dispersion in $SrTiO_3$ by broadband stimulated Brillouin scattering" [Appl. Phys. Lett. 98 (2011) 211907]. *Appl. Phys. Lett.* **2012**, *100*, No. 206101.
(16) Rivas, N.; Zhong, S.; Dekker, T.; Cheng, M.; Gicala, P.; Chen, F.; Luo, X.; Sun, Y.; Petruk, A. A.; Pichugin, K.; Tsen, A. W.; Sciaini, G. Generation and detection of coherent longitudinal acoustic waves in ultrathin 1T'-$MoTe_2$. *Appl. Phys. Lett.* **2019**, *115*, No. 223103.
(17) Huang, W.; Wang, M.; Hu, L.; Wang, C.; Xie, Z.; Zhang, H. Recent Advances in Semiconducting Monoelemental Selenium Nanostructures for Device Applications. *Adv. Funct. Mater.* **2020**, *30*, No. 2003301.
(18) Huang, W.; Zhu, J.; Wang, M.; Hu, L.; Tang, Y.; Shu, Y.; Xie, Z.; Zhang, H. Emerging Mono-Elemental Bismuth Nanostructures: Controlled Synthesis and Their Versatile Applications. *Adv. Funct. Mater.* **2021**, *31* (10), No. 2007584, DOI: 10.1002/adfm.202007584.
(19) Zi, Y.; Zhu, J.; Hu, L.; Wang, M.; Huang, W. Nanoengineering of Tin Monosulfide (SnS)-Based Structures for Emerging Applications. *Small Sci.* **2022**, *2*, No. 2100098.
(20) Hu, Y.; Wang, M.; Hu, L.; Hu, Y.; Guo, J.; Xie, Z.; Wei, S.; Wang, Y.; Zi, Y.; Zhang, H.; Wang, Q.; Huang, W. Recent Advances in Two-Dimensional Graphdiyne for Nanophotonic Applications. *Chem. Eng. J.* **2022**, *450*, No. 138228.
(21) Chiao, R. Y.; Townes, C. H.; Stoicheff, B. P. Stimulated Brillouin Scattering and Coherent Generation of Intense Hypersonic Waves. *Phys. Rev. Lett.* **1964**, *12* (21), 592−595.
(22) Ballmann, C. W.; Meng, Z.; Traverso, A. J.; Scully, M. O.; Yakovlev, V. V. Impulsive Brillouin microscopy. *Optica* **2017**, *4*, 124−128.
(23) Krug, B.; Koukourakis, N.; Czarske, J. W. Impulsive stimulated Brillouin microscopy for non-contact, fast mechanical investigations of hydrogels. *Opt. Express* **2019**, *27*, 26910−26923.
(24) Gicala, P.; Cheng, M.; Lott, T. S.; Du, K.; Cheong, S.-W.; Petruk, A. A.; Pichugin, K.; Sciaini, G. Time-resolved broadband impulsive stimulated Brillouin scattering in single crystal hematite. *Appl. Phys. Lett.* **2021**, *118*, No. 264101.
(25) Krug, B.; Koukourakis, N.; Guck, J.; Czarske, J. W. Nonlinear microscopy using impulsive stimulated Brillouin scattering for high-speed elastography. *Opt. Express* **2022**, *30*, 4748−4758.
(26) O'Connor, S. P.; Doktor, D. A.; Scully, M. O.; Yakovlev, V. V. Spectral resolution enhancement for impulsive stimulated Brillouin spectroscopy by expanding pump beam geometry. *Opt. Express* **2023**, *31*, 14604−14616.
(27) Lin, H.-N.; Stoner, R. J.; Maris, H. J.; Tauc, J. Phonon attenuation and velocity measurements in transparent materials by picosecond acoustic interferometry. *J. Appl. Phys.* **1991**, *69*, 3816−3822.
(28) Wang, Y.; Hurley, D. H.; Hua, Z.; Pezeril, T.; Raetz, S.; Gusev, V. E.; Tournat, V.; Khafizov, M. Imaging grain microstructure in a model ceramic energy material with optically generated coherent acoustic phonons. *Nat. Commun.* **2020**, *11*, No. 1597, DOI: 10.1038/s41467-020-15360-3.
(29) Gusev, V. E. Contra-intuitive features of time-domain Brillouin scattering in collinear paraxial sound and light beams. *Photoacoustics* **2020**, *20*, No. 100205.
(30) Zhang, X.; Song, H.-Y.; Nie, X. C.; Liu, S.-B.; Wang, Y.; Jiang, C.-Y.; Zhao, S.-Z.; Chen, G.; Meng, J.-Q.; Duan, Y.-X.; Liu, H. Y. Ultrafast hot carrier dynamics of $ZrTe_5$ from time-resolved optical reflectivity. *Phys. Rev. B* **2019**, *99*, No. 125141.
(31) Tan, D.; Lim, H. E.; Wang, F.; Mohamed, N. B.; Mouri, S.; Zhang, W.; Miyauchi, Y.; Ohfuchi, M.; Matsuda, K. Anisotropic optical and electronic properties of two-dimensional layered germanium sulfide. *Nano Res.* **2017**, *10*, 546−555.
(32) Solís-Vivanco, J. F.; De Moure-Flores, F.; Arenas-Arrocena, M. C.; Santos-Cruz, J. Effect in the power conversion efficiency in inverted P3HT organic solar cells doped with nano germanium sulfide. *J. Mater. Res.* **2023**, *38*, 2413−2421.
(33) Lan, C.; Li, C.; Yin, Y.; Guoa, H.; Wang, S. Synthesis of single-crystalline GeS nanoribbons for high sensitivity visible-light photodetectors. *J. Mater. Chem. C* **2015**, *3*, 8074−8079.
(34) Ramasamy, P.; Kwak, D.; Lim, D.-H.; Raa, H.-S.; Lee, J.-S. Solution synthesis of GeS and GeSe nanosheets for high-sensitivity photodetectors. *J. Mater. Chem. C* **2016**, *4*, 479−485.
(35) Ma, S.; Yuan, D.; Wang, Y.; Jiao, Z. Monolayer GeS as a potential candidate for NO_2 gas sensors and capturers. *J. Mater. Chem. C* **2018**, *6*, 8082−8091.
(36) Gao, R.; Yong, Y.; Hu, S.; Zhao, Z.; Li, X.; Kuang, Y. Adsorption and gas-sensing performance of SF_6 decomposition gases on GeS monolayers with and without single vacancies and Si-doping. *Appl. Surf. Sci.* **2021**, *568*, No. 150961.
(37) Li, C.; Xu, X.; Song, T.; Zhu, X.; Li, Y.; Jia, H.; Liu, Y. Fabrication of GeS-graphene composites for electrode materials in lithium-ion batteries. *Mater. Res. Express* **2021**, *8*, No. 115013.
(38) Boland, J. B.; Tian, R.; Harvey, A.; Vega-Mayoral, V.; Griffin, A.; Horvath, D. V.; Gabbett, C.; Breshears, M.; Pepper, J.; Li, Y.; Coleman, J. N. Liquid phase exfoliation of GeS nanosheets in ambient conditions for lithium ion battery applications. *2D Mater.* **2020**, *7*, No. 035015, DOI: 10.1088/2053-1583/ab89e6.
(39) Sutter, E.; Sutter, P. 1D wires of 2D layered materials: germanium sulfide nanowires as efficient light emitters. *ACS Appl. Nano Mater.* **2018**, *1*, 1042−1049.
(40) Li, C.; Huang, L.; Snigdha, G. P.; Yu, Y.; Cao, L. Role of boundary layer diffusion in vapor deposition growth of chalcogenide nanosheets: the case of GeS. *ACS Nano* **2012**, *6*, 8868−8877.
(41) Zhang, Q.; Matsumura, R.; Fukata, N. Synthesis of Large-Area GeS Thin Films with the Assistance of Pre-deposited Amorphous Nanostructured GeS Films: Implications for Electronic and Optoelectronic Applications. *ACS Appl. Nano Mater.* **2023**, *6*, 6920−6928.
(42) Guo, Y.; Zhou, S.; Bai, Y.; Zhao, J. Oxidation Resistance of Monolayer Group-IV Monochalcogenides. *ACS Appl. Mater. Interfaces* **2017**, *9*, 12013−12020.
(43) Yu, D.; Ku, R.; Hu, Y.; Wei, Y.; Zhu, C.; Liu, Z.; Zhang, G.; Li, W.; Yang, J.; Li, X. Prediction of the electronic structure of single-walled GeS nanotubes. *RSC Adv.* **2022**, *12*, 29291−29299.
(44) Zachariasen, W. H. The crystal lattice of Germano Sulphide, GeS. *Phys. Rev.* **1932**, *40*, 917.
(45) Vargas-Bernal, R. Electrical properties of two-dimensional materials used in gas sensors. *Sensors* **2019**, *19*, 1295.
(46) Lejman, M.; Vaudel, G.; Infante, I. C.; Gemeiner, P.; Gusev, V. E.; Dkhil, B.; Ruello, P. Giant ultrafast photo-induced shear strain in ferroelectric $BiFeO_3$. *Nat. Commun.* **2014**, *5*, No. 4301.
(47) Chang, P. C. Y.; Walker, J. G.; Hopcraft, K. I. Ray tracing in absorbing media. *J. Quant. Spectrosc. Radiat. Transfer* **2005**, *96*, 327−341.
(48) Koc, H.; Simsek, S.; Palaz, S.; Oltulu, O.; Mamedov, A. M.; Ozbay, E. Mechanical, electronic, and opticalproperties of the A_4B_6 layered ferroelectrics:ab initio calculation. *Phys. Status Solidi C* **2015**, *12*, 651−658.
(49) Cheng, M.; Pichugin, K.; Maas, A.; Schleberger, M.; Sciaini, G. Out-of-plane longitudinal sound velocity in SnS_2 determined via broadband time-domain Brillouin scattering. *J. Appl. Phys.* **2022**, *132*, No. 075107.
(50) Zhen, Z.-Q.; Wang, H.-Y. *Acta Phys. Pol., A* **2020**, *137*, 1095−1100.

NOTE ADDED AFTER ASAP PUBLICATION

This paper orginally published ASAP on March 12, 2024. Due to a production error, equation 1 was incorrect and a new version reposted on March 18, 2024.

https://doi.org/10.1021/acsomega.4c00266
ACS Omega 2024, 9, 15463−15467